

Study of $\chi_{bJ}(1P)$ Properties in the Radiative $\Upsilon(2S)$ Decays

A. Abdesselam,⁹² I. Adachi,^{20,16} K. Adamczyk,⁶⁶ H. Aihara,¹⁰⁰ S. Al Said,^{92,42} K. Arinstein,^{5,70} Y. Arita,⁵⁹
D. M. Asner,⁷³ T. Aso,¹⁰⁵ H. Atmacan,⁵⁵ V. Aulchenko,^{5,70} T. Aushev,⁵⁸ R. Ayad,⁹² T. Aziz,⁹³ V. Babu,⁹³
I. Badhrees,^{92,41} S. Bahinipati,²⁶ A. M. Bakich,⁹¹ A. Bala,⁷⁴ Y. Ban,⁷⁵ V. Bansal,⁷³ E. Barberio,⁵⁴
M. Barrett,¹⁹ W. Bartel,¹⁰ A. Bay,⁴⁷ I. Bedny,^{5,70} P. Behera,²⁸ M. Belhorn,⁹ K. Belous,³² M. Berger,⁸⁹
D. Besson,⁵⁷ V. Bhardwaj,²⁵ B. Bhuyan,²⁷ J. Biswal,³⁶ T. Bloomfield,⁵⁴ S. Blyth,⁶⁴ A. Bobrov,^{5,70} A. Bondar,^{5,70}
G. Bonvicini,¹⁰⁸ C. Bookwalter,⁷³ C. Boulahouache,⁹² A. Bozek,⁶⁶ M. Bračko,^{52,36} F. Breibeck,³¹ J. Brodzicka,⁶⁶
T. E. Browder,¹⁹ E. Waheed,⁵⁴ D. Červenkov,⁶ M.-C. Chang,¹² P. Chang,⁶⁵ Y. Chao,⁶⁵ V. Chekelian,⁵³ A. Chen,⁶³
K.-F. Chen,⁶⁵ P. Chen,⁶⁵ B. G. Cheon,¹⁸ K. Chilikin,^{48,57} R. Chistov,^{48,57} K. Cho,⁴³ V. Chobanova,⁵³ S.-K. Choi,¹⁷
Y. Choi,⁹⁰ D. Cinabro,¹⁰⁸ J. Crnkovic,²⁴ J. Dalseno,^{53,94} M. Danilov,^{57,48} N. Dash,²⁶ S. Di Carlo,¹⁰⁸ J. Dingfelder,⁴
Z. Doležal,⁶ D. Dossett,⁵⁴ Z. Drásal,⁶ A. Drutskoy,^{48,57} S. Dubey,¹⁹ D. Dutta,⁹³ K. Dutta,²⁷ S. Eidelman,^{5,70}
D. Epifanov,¹⁰⁰ S. Esen,⁹ H. Farhat,¹⁰⁸ J. E. Fast,⁷³ M. Feindt,³⁸ T. Ferber,¹⁰ A. Frey,¹⁵ O. Frost,¹⁰ B. G. Fulsom,⁷³
V. Gaur,⁹³ N. Gabyshev,^{5,70} S. Ganguly,¹⁰⁸ A. Garmash,^{5,70} D. Getzkow,¹³ R. Gillard,¹⁰⁸ F. Giordano,²⁴
R. Glattauer,³¹ Y. M. Goh,¹⁸ P. Goldenzweig,³⁸ B. Golob,^{49,36} D. Greenwald,⁹⁵ M. Grosse Perdekamp,^{24,81}
J. Grygier,³⁸ O. Grzymkowska,⁶⁶ H. Guo,⁸³ J. Haba,^{20,16} P. Hamer,¹⁵ Y. L. Han,³⁰ K. Hara,²⁰ T. Hara,^{20,16}
Y. Hasegawa,⁸⁵ J. Hasenbusch,⁴ K. Hayasaka,⁶⁸ H. Hayashii,⁶² X. H. He,⁷⁵ M. Heck,³⁸ M. T. Hedges,¹⁹
D. Heffernan,⁷² M. Heider,³⁸ A. Heller,³⁸ T. Higuchi,³⁹ S. Himori,⁵⁹ S. Hirose,⁵⁹ T. Horiguchi,⁹⁸ Y. Hoshi,⁹⁷
K. Hoshina,¹⁰³ W.-S. Hou,⁶⁵ Y. B. Hsiung,⁶⁵ C.-L. Hsu,⁵⁴ M. Huschle,³⁸ H. J. Hyun,⁴⁶ Y. Igarashi,²⁰ T. Iijima,^{60,59}
M. Imamura,⁵⁹ K. Inami,⁵⁹ G. Inguglia,¹⁰ A. Ishikawa,⁹⁸ K. Itagaki,⁹⁸ R. Itoh,^{20,16} M. Iwabuchi,¹¹⁰ M. Iwasaki,¹⁰⁰
Y. Iwasaki,²⁰ S. Iwata,¹⁰² W. W. Jacobs,²⁹ I. Jaegle,¹⁹ H. B. Jeon,⁴⁶ D. Joffe,⁴⁰ M. Jones,¹⁹ K. K. Joo,⁸ T. Julius,⁵⁴
H. Kakuno,¹⁰² J. H. Kang,¹¹⁰ K. H. Kang,⁴⁶ P. Kapusta,⁶⁶ S. U. Kataoka,⁶¹ E. Kato,⁹⁸ Y. Kato,⁵⁹ P. Katrenko,^{58,48}
H. Kawai,⁷ T. Kawasaki,⁶⁸ T. Keck,³⁸ H. Kichimi,²⁰ C. Kiesling,⁵³ B. H. Kim,⁸⁴ D. Y. Kim,⁸⁷ H. J. Kim,⁴⁶
H.-J. Kim,¹¹⁰ J. B. Kim,⁴⁴ J. H. Kim,⁴³ K. T. Kim,⁴⁴ M. J. Kim,⁴⁶ S. H. Kim,¹⁸ S. K. Kim,⁸⁴ Y. J. Kim,⁴³
K. Kinoshita,⁹ C. Kleinwort,¹⁰ J. Klucar,³⁶ B. R. Ko,⁴⁴ N. Kobayashi,¹⁰¹ S. Koblitz,⁵³ P. Kodyš,⁶ Y. Koga,⁵⁹
S. Korpar,^{52,36} D. Kotchetkov,¹⁹ R. T. Kouzes,⁷³ P. Križan,^{49,36} P. Krokovny,^{5,70} B. Kronenbitter,³⁸ T. Kuhr,⁵⁰
R. Kumar,⁷⁷ T. Kumita,¹⁰² E. Kurihara,⁷ Y. Kuroki,⁷² A. Kuzmin,^{5,70} P. Kvasnička,⁶ Y.-J. Kwon,¹¹⁰ Y.-T. Lai,⁶⁵
J. S. Lange,¹³ D. H. Lee,⁴⁴ I. S. Lee,¹⁸ S.-H. Lee,⁴⁴ M. Leitgab,^{24,81} R. Leitner,⁶ D. Levit,⁹⁵ P. Lewis,¹⁹ C. H. Li,⁵⁴
H. Li,²⁹ J. Li,⁸⁴ L. Li,⁸³ X. Li,⁸⁴ Y. Li,¹⁰⁷ L. Li Gioi,⁵³ J. Libby,²⁸ A. Limosani,⁵⁴ C. Liu,⁸³ Y. Liu,⁹ Z. Q. Liu,³⁰
D. Liventsev,^{107,20} A. Loos,⁸⁸ R. Louvot,⁴⁷ M. Lubej,³⁶ P. Lukin,^{5,70} T. Luo,⁷⁶ J. MacNaughton,²⁰ M. Masuda,⁹⁹
T. Matsuda,⁵⁶ D. Matvienko,^{5,70} A. Matyja,⁶⁶ S. McOnie,⁹¹ Y. Mikami,⁹⁸ K. Miyabayashi,⁶² Y. Miyachi,¹⁰⁹
H. Miyake,^{20,16} H. Miyata,⁶⁸ Y. Miyazaki,⁵⁹ R. Mizuk,^{48,57,58} G. B. Mohanty,⁹³ S. Mohanty,^{93,106} D. Mohapatra,⁷³
A. Moll,^{53,94} H. K. Moon,⁴⁴ T. Mori,⁵⁹ T. Morii,³⁹ H.-G. Moser,⁵³ T. Müller,³⁸ N. Muramatsu,⁷⁸ R. Mussa,³⁴
T. Nagamine,⁹⁸ Y. Nagasaka,²² Y. Nakahama,¹⁰⁰ I. Nakamura,^{20,16} K. R. Nakamura,²⁰ E. Nakano,⁷¹ H. Nakano,⁹⁸
T. Nakano,⁷⁹ M. Nakao,^{20,16} H. Nakayama,^{20,16} H. Nakazawa,⁶³ T. Nanut,³⁶ K. J. Nath,²⁷ Z. Natkaniec,⁶⁶
M. Nayak,^{108,20} E. Nedelkovska,⁵³ K. Negishi,⁹⁸ K. Neichi,⁹⁷ C. Ng,¹⁰⁰ C. Niebuhr,¹⁰ M. Niiyama,⁴⁵ N. K. Nisar,^{93,1}
S. Nishida,^{20,16} K. Nishimura,¹⁹ O. Nitoh,¹⁰³ T. Nozaki,²⁰ A. Ogawa,⁸¹ S. Ogawa,⁹⁶ T. Ohshima,⁵⁹ S. Okuno,³⁷
S. L. Olsen,⁸⁴ Y. Ono,⁹⁸ Y. Onuki,¹⁰⁰ W. Ostrowicz,⁶⁶ C. Oswald,⁴ H. Ozaki,^{20,16} P. Pakhlov,^{48,57} G. Pakhlova,^{48,58}
B. Pal,⁹ H. Palka,⁶⁶ E. Panzenböck,^{15,62} C.-S. Park,¹¹⁰ C. W. Park,⁹⁰ H. Park,⁴⁶ K. S. Park,⁹⁰ S. Paul,⁹⁵
L. S. Peak,⁹¹ T. K. Pedlar,⁵¹ T. Peng,⁸³ L. Pesántez,⁴ R. Pestotnik,³⁶ M. Peters,¹⁹ M. Petrič,³⁶ L. E. Pilonen,¹⁰⁷
A. Poluektov,^{5,70} K. Prasanth,²⁸ M. Prim,³⁸ K. Prothmann,^{53,94} C. Pulvermacher,³⁸ M. V. Purohit,⁸⁸ J. Rauch,⁹⁵
B. Reisert,⁵³ E. Ribežl,³⁶ M. Ritter,⁵⁰ M. Röhrken,³⁸ J. Rorie,¹⁹ A. Rostomyan,¹⁰ M. Rozanska,⁶⁶ S. Rummel,⁵⁰
S. Ryu,⁸⁴ H. Sahoo,¹⁹ T. Saito,⁹⁸ K. Sakai,²⁰ Y. Sakai,^{20,16} S. Sandilya,⁹ D. Santel,⁹ L. Santelj,²⁰ T. Sanuki,⁹⁸
N. Sasao,⁴⁵ Y. Sato,⁵⁹ V. Savinov,⁷⁶ T. Schlüter,⁵⁰ O. Schneider,⁴⁷ G. Schnell,^{2,23} P. Schönmeier,⁹⁸ M. Schram,⁷³
C. Schwanda,³¹ A. J. Schwartz,⁹ B. Schwenker,¹⁵ R. Seidl,⁸¹ Y. Seino,⁶⁸ D. Semmler,¹³ K. Senyo,¹⁰⁹ O. Seon,⁵⁹
I. S. Seong,¹⁹ M. E. Sevier,⁵⁴ L. Shang,³⁰ M. Shapkin,³² V. Shebalin,^{5,70} C. P. Shen,³ T.-A. Shibata,¹⁰¹
H. Shibuya,⁹⁶ S. Shinomiya,⁷² J.-G. Shiu,⁶⁵ B. Shwartz,^{5,70} A. Sibidanov,⁹¹ F. Simon,^{53,94} J. B. Singh,⁷⁴ R. Sinha,³³
P. Smerkol,³⁶ Y.-S. Sohn,¹¹⁰ A. Sokolov,³² Y. Soloviev,¹⁰ E. Solovieva,^{48,58} S. Stanič,⁶⁹ M. Starič,³⁶ M. Steder,¹⁰
J. F. Strube,⁷³ J. Stypula,⁶⁶ S. Sugihara,¹⁰⁰ A. Sugiyama,⁸² M. Sumihama,¹⁴ K. Sumisawa,^{20,16} T. Sumiyoshi,¹⁰²
K. Suzuki,⁵⁹ K. Suzuki,⁸⁹ S. Suzuki,⁸² S. Y. Suzuki,²⁰ Z. Suzuki,⁹⁸ H. Takeichi,⁵⁹ M. Takizawa,^{86,21,80}

U. Tamponi,^{34, 104} M. Tanaka,^{20, 16} S. Tanaka,^{20, 16} K. Tanida,³⁵ N. Taniguchi,²⁰ G. N. Taylor,⁵⁴ F. Tenchini,⁵⁴ Y. Teramoto,⁷¹ I. Tikhomirov,⁵⁷ K. Trabelsi,^{20, 16} V. Trusov,³⁸ Y. F. Tse,⁵⁴ T. Tsuboyama,^{20, 16} M. Uchida,¹⁰¹ T. Uchida,²⁰ S. Uehara,^{20, 16} K. Ueno,⁶⁵ T. Uglov,^{48, 58} Y. Unno,¹⁸ S. Uno,^{20, 16} S. Uozumi,⁴⁶ P. Urquijo,⁵⁴ Y. Ushiroda,^{20, 16} Y. Usov,^{5, 70} S. E. Vahsen,¹⁹ C. Van Hulse,² P. Vanhoefer,⁵³ G. Varner,¹⁹ K. E. Varvell,⁹¹ K. Vervink,⁴⁷ A. Vinokurova,^{5, 70} V. Vorobyev,^{5, 70} A. Vossen,²⁹ M. N. Wagner,¹³ E. Waheed,⁵⁴ C. H. Wang,⁶⁴ J. Wang,⁷⁵ M.-Z. Wang,⁶⁵ P. Wang,³⁰ X. L. Wang,^{73, 20} M. Watanabe,⁶⁸ Y. Watanabe,³⁷ R. Wedd,⁵⁴ S. Wehle,¹⁰ E. White,⁹ E. Widmann,⁸⁹ J. Wiechczynski,⁶⁶ K. M. Williams,¹⁰⁷ E. Won,⁴⁴ B. D. Yabsley,⁹¹ S. Yamada,²⁰ H. Yamamoto,⁹⁸ J. Yamaoka,⁷³ Y. Yamashita,⁶⁷ M. Yamauchi,^{20, 16} S. Yashchenko,¹⁰ H. Ye,¹⁰ J. Yelton,¹¹ Y. Yook,¹¹⁰ C. Z. Yuan,³⁰ Y. Yusa,⁶⁸ C. C. Zhang,³⁰ L. M. Zhang,⁸³ Z. P. Zhang,⁸³ L. Zhao,⁸³ V. Zhilich,^{5, 70} V. Zhukova,⁵⁷ V. Zhulanov,^{5, 70} M. Ziegler,³⁸ T. Zivko,³⁶ A. Zupanc,^{49, 36} N. Zwahlen,⁴⁷ and O. Zyukova,^{5, 70}

(The Belle Collaboration)

¹Aligarh Muslim University, Aligarh 202002

²University of the Basque Country UPV/EHU, 48080 Bilbao

³Beihang University, Beijing 100191

⁴University of Bonn, 53115 Bonn

⁵Budker Institute of Nuclear Physics SB RAS, Novosibirsk 630090

⁶Faculty of Mathematics and Physics, Charles University, 121 16 Prague

⁷Chiba University, Chiba 263-8522

⁸Chonnam National University, Kwangju 660-701

⁹University of Cincinnati, Cincinnati, Ohio 45221

¹⁰Deutsches Elektronen-Synchrotron, 22607 Hamburg

¹¹University of Florida, Gainesville, Florida 32611

¹²Department of Physics, Fu Jen Catholic University, Taipei 24205

¹³Justus-Liebig-Universität Gießen, 35392 Gießen

¹⁴Gifu University, Gifu 501-1193

¹⁵II. Physikalisches Institut, Georg-August-Universität Göttingen, 37073 Göttingen

¹⁶SOKENDAI (The Graduate University for Advanced Studies), Hayama 240-0193

¹⁷Gyeongsang National University, Chinju 660-701

¹⁸Hanyang University, Seoul 133-791

¹⁹University of Hawaii, Honolulu, Hawaii 96822

²⁰High Energy Accelerator Research Organization (KEK), Tsukuba 305-0801

²¹J-PARC Branch, KEK Theory Center, High Energy Accelerator Research Organization (KEK), Tsukuba 305-0801

²²Hiroshima Institute of Technology, Hiroshima 731-5193

²³IKERBASQUE, Basque Foundation for Science, 48013 Bilbao

²⁴University of Illinois at Urbana-Champaign, Urbana, Illinois 61801

²⁵Indian Institute of Science Education and Research Mohali, SAS Nagar, 140306

²⁶Indian Institute of Technology Bhubaneswar, Satya Nagar 751007

²⁷Indian Institute of Technology Guwahati, Assam 781039

²⁸Indian Institute of Technology Madras, Chennai 600036

²⁹Indiana University, Bloomington, Indiana 47408

³⁰Institute of High Energy Physics, Chinese Academy of Sciences, Beijing 100049

³¹Institute of High Energy Physics, Vienna 1050

³²Institute for High Energy Physics, Protvino 142281

³³Institute of Mathematical Sciences, Chennai 600113

³⁴INFN - Sezione di Torino, 10125 Torino

³⁵Advanced Science Research Center, Japan Atomic Energy Agency, Naka 319-1195

³⁶J. Stefan Institute, 1000 Ljubljana

³⁷Kanagawa University, Yokohama 221-8686

³⁸Institut für Experimentelle Kernphysik, Karlsruher Institut für Technologie, 76131 Karlsruhe

³⁹Kavli Institute for the Physics and Mathematics of the Universe (WPI), University of Tokyo, Kashiwa 277-8583

⁴⁰Kennesaw State University, Kennesaw, Georgia 30144

⁴¹King Abdulaziz City for Science and Technology, Riyadh 11442

⁴²Department of Physics, Faculty of Science, King Abdulaziz University, Jeddah 21589

⁴³Korea Institute of Science and Technology Information, Daejeon 305-806

⁴⁴Korea University, Seoul 136-713

⁴⁵Kyoto University, Kyoto 606-8502

⁴⁶Kyungpook National University, Daegu 702-701

⁴⁷École Polytechnique Fédérale de Lausanne (EPFL), Lausanne 1015

⁴⁸P.N. Lebedev Physical Institute of the Russian Academy of Sciences, Moscow 119991

⁴⁹Faculty of Mathematics and Physics, University of Ljubljana, 1000 Ljubljana

⁵⁰Ludwig Maximilians University, 80539 Munich

- ⁵¹Luther College, Decorah, Iowa 52101
- ⁵²University of Maribor, 2000 Maribor
- ⁵³Max-Planck-Institut für Physik, 80805 München
- ⁵⁴School of Physics, University of Melbourne, Victoria 3010
- ⁵⁵Middle East Technical University, 06531 Ankara
- ⁵⁶University of Miyazaki, Miyazaki 889-2192
- ⁵⁷Moscow Physical Engineering Institute, Moscow 115409
- ⁵⁸Moscow Institute of Physics and Technology, Moscow Region 141700
- ⁵⁹Graduate School of Science, Nagoya University, Nagoya 464-8602
- ⁶⁰Kobayashi-Maskawa Institute, Nagoya University, Nagoya 464-8602
- ⁶¹Nara University of Education, Nara 630-8528
- ⁶²Nara Women's University, Nara 630-8506
- ⁶³National Central University, Chung-li 32054
- ⁶⁴National United University, Miao Li 36003
- ⁶⁵Department of Physics, National Taiwan University, Taipei 10617
- ⁶⁶H. Niewodniczanski Institute of Nuclear Physics, Krakow 31-342
- ⁶⁷Nippon Dental University, Niigata 951-8580
- ⁶⁸Niigata University, Niigata 950-2181
- ⁶⁹University of Nova Gorica, 5000 Nova Gorica
- ⁷⁰Novosibirsk State University, Novosibirsk 630090
- ⁷¹Osaka City University, Osaka 558-8585
- ⁷²Osaka University, Osaka 565-0871
- ⁷³Pacific Northwest National Laboratory, Richland, Washington 99352
- ⁷⁴Panjab University, Chandigarh 160014
- ⁷⁵Peking University, Beijing 100871
- ⁷⁶University of Pittsburgh, Pittsburgh, Pennsylvania 15260
- ⁷⁷Punjab Agricultural University, Ludhiana 141004
- ⁷⁸Research Center for Electron Photon Science, Tohoku University, Sendai 980-8578
- ⁷⁹Research Center for Nuclear Physics, Osaka University, Osaka 567-0047
- ⁸⁰Theoretical Research Division, Nishina Center, RIKEN, Saitama 351-0198
- ⁸¹RIKEN BNL Research Center, Upton, New York 11973
- ⁸²Saga University, Saga 840-8502
- ⁸³University of Science and Technology of China, Hefei 230026
- ⁸⁴Seoul National University, Seoul 151-742
- ⁸⁵Shinshu University, Nagano 390-8621
- ⁸⁶Showa Pharmaceutical University, Tokyo 194-8543
- ⁸⁷Soongsil University, Seoul 156-743
- ⁸⁸University of South Carolina, Columbia, South Carolina 29208
- ⁸⁹Stefan Meyer Institute for Subatomic Physics, Vienna 1090
- ⁹⁰Sungkyunkwan University, Suwon 440-746
- ⁹¹School of Physics, University of Sydney, New South Wales 2006
- ⁹²Department of Physics, Faculty of Science, University of Tabuk, Tabuk 71451
- ⁹³Tata Institute of Fundamental Research, Mumbai 400005
- ⁹⁴Excellence Cluster Universe, Technische Universität München, 85748 Garching
- ⁹⁵Department of Physics, Technische Universität München, 85748 Garching
- ⁹⁶Toho University, Funabashi 274-8510
- ⁹⁷Tohoku Gakuin University, Tagajo 985-8537
- ⁹⁸Department of Physics, Tohoku University, Sendai 980-8578
- ⁹⁹Earthquake Research Institute, University of Tokyo, Tokyo 113-0032
- ¹⁰⁰Department of Physics, University of Tokyo, Tokyo 113-0033
- ¹⁰¹Tokyo Institute of Technology, Tokyo 152-8550
- ¹⁰²Tokyo Metropolitan University, Tokyo 192-0397
- ¹⁰³Tokyo University of Agriculture and Technology, Tokyo 184-8588
- ¹⁰⁴University of Torino, 10124 Torino
- ¹⁰⁵Toyama National College of Maritime Technology, Toyama 933-0293
- ¹⁰⁶Utkal University, Bhubaneswar 751004
- ¹⁰⁷Virginia Polytechnic Institute and State University, Blacksburg, Virginia 24061
- ¹⁰⁸Wayne State University, Detroit, Michigan 48202
- ¹⁰⁹Yamagata University, Yamagata 990-8560
- ¹¹⁰Yonsei University, Seoul 120-749

We report a study of radiative decays of $\chi_{bJ}(1P)$ ($J = 0, 1, 2$) mesons into 74 hadronic final states comprising charged and neutral pions, kaons, protons; out of these, 41 modes are observed with at least 5 standard deviation significance. Our measurements not only improve the previous

measurements by the CLEO Collaboration but also lead to first observations in many new modes. The large sample allows us to probe the total decay width of the $\chi_{b0}(1P)$. In the absence of a statistically significant result, a 90% confidence-level upper limit is set on the width at $\Gamma_{\text{total}} < 2.4 \text{ MeV}$. Our results are based on 24.7 fb^{-1} of e^+e^- collision data recorded by the Belle detector at the $\Upsilon(2S)$ resonance, corresponding to $(157.8 \pm 3.6) \times 10^6$ $\Upsilon(2S)$ decays.

PACS numbers: 14.40.Pq, 13.25.Gv, 12.39.Pn

I. INTRODUCTION

The P -wave spin triplet states of bottomonia, $\chi_{bJ}(nP)$, are copiously produced from the $\Upsilon(nS)$ states through electric dipole radiative transitions. The $\chi_{b0}(1P)$ and $\chi_{b2}(1P)$ states, with positive parity and charge-parity, can annihilate to two real photons or gluons. Various theoretical predictions for the two-gluon widths ($\Gamma_{\text{total}} \approx \Gamma_{2g}$) of the $\chi_{b0}(1P)$ ($J^{\text{PC}} = 0^{++}$) and $\chi_{b2}(1P)$ ($J^{\text{PC}} = 2^{++}$) states are listed in Table I. All calculations predict the width of $\chi_{b0}(1P)$ to be larger than that of $\chi_{b2}(1P)$, reaching above 2 MeV. On the experimental front, so far there is no measurement for the width of any of the $\chi_{bJ}(1P)$ states. According to the Landau-Yang theorem [1], a $J = 1$ particle cannot decay to two identical massless spin-1 particles, thus the $\chi_{b1}(1P)$ cannot decay to two real gluons or photons. However, this process is allowed if one of the gluons is virtual giving rise to a quark-antiquark pair [2].

In 2008, the CLEO Collaboration reported the first observations of $\chi_{bJ}(1P)$ and $\chi_{bJ}(2P)$ decays into specific final states of light hadrons, where these P -wave states are produced in radiative transitions of the $\Upsilon(2S)$ and $\Upsilon(3S)$ resonances, respectively [11]. In our earlier search for a new state near $9975 \text{ MeV}/c^2$, $X_{bb}(9975)$ [12], we observed a large signal yield for $\chi_{bJ}(1P)$ states from the sum of 26 exclusive hadronic final states. The yields for $\chi_{bJ}(1P)$ ($J = 0, 1, 2$) were 299 ± 22 , 946 ± 36 and 582 ± 31 , respectively. This motivated a study of the product branching fractions $\mathcal{B}[\Upsilon(2S) \rightarrow \gamma\chi_{bJ}(1P)] \times \mathcal{B}[\chi_{bJ}(1P) \rightarrow h_i]$, where h_i is a specific hadronic mode; such decays of $\chi_{bJ}(1P)$ mesons give us insight into how initial quarks and gluons hadronize [13]. Our study, using the world's largest $e^+e^- \rightarrow \Upsilon(2S)$ data sample, permits us not only to improve upon the earlier measurements of 14 modes [11], but also to uncover many new modes. The analysis also provides an opportunity for a width measurement of $\chi_{b0}(1P)$, which is predicted to be the largest among the three $\chi_{bJ}(1P)$ states.

II. DATA AND SIMULATION SAMPLES

We perform this study using a 24.7 fb^{-1} data sample, equivalent to $(157.8 \pm 3.6) \times 10^6$ $\Upsilon(2S)$ events [14], collected at the $\Upsilon(2S)$ resonance with the Belle detector [15] at the KEKB asymmetric-energy e^+e^- collider [16]. A 1.7 fb^{-1} data sample, recorded 30 MeV below the $\Upsilon(2S)$ peak, provides a control sample to study the $e^+e^- \rightarrow q\bar{q}$ ($q = u, d, s, c$) continuum background.

TABLE I: Predicted total widths (in keV) of the $\chi_{b0}(1P)$ and $\chi_{b2}(1P)$ states, assuming $\Gamma_{\text{total}} \approx \Gamma_{2g}$.

$\Gamma[\chi_{b0}(1P)]$ (keV)	$\Gamma[\chi_{b2}(1P)]$ (keV)	Ref.
2.03 (MeV)	122.84	[3]
431^{+45}_{-49}	214^{+1}_{-0}	[4]
887	220	[5, 6]
960 (2740)	330 (250)	[4, 7]
653	109	[8]
2150 (2290)	220 (330)	[9]
672	123	[10]

The values of [7] are obtained by the perturbative (non-perturbative) calculation and that for [9] are obtained by the QCD potential (alternative treatment)

Half a million signal Monte Carlo (MC) events are produced for each final state studied. The radiative transitions from the $\Upsilon(2S)$ are generated using the helicity amplitude formalism [17]. Hadronic decays of χ_{bJ} are modeled assuming a phase space distribution, where an interface to PHOTOS [18] has been added to incorporate final state radiation effects. As all signal MC samples are generated with a phase space distribution, possible intermediate decays such as $\rho^0 \rightarrow \pi^+\pi^-$, $\rho^\pm \rightarrow \pi^\pm\pi^0$, $\phi \rightarrow K^+K^-$, $\omega \rightarrow \pi^+\pi^-\pi^0$, $\bar{K}^{*0}(892)^0 \rightarrow K^\pm\pi^\mp/K_s^0\pi^0$ and $K^{*0}(892)^0 \rightarrow K_s^0\pi^\pm/K^\pm\pi^0$ are considered primarily when we later estimate systematic uncertainties in efficiency. Inclusive $\Upsilon(2S)$ MC events, produced using PYTHIA [19] with the same luminosity as the data, are utilized for background studies.

III. EXPERIMENTAL APPARATUS

The Belle detector [15] is a large-solid-angle magnetic spectrometer consisting of a silicon vertex detector, a 50-layer central drift chamber (CDC), an array of aerogel threshold Cherenkov counters (ACC), a barrel-like arrangement of time-of-flight scintillation counters (TOF), and an electromagnetic calorimeter comprised of CsI(Tl) crystals (ECL). All these detector elements are located inside a superconducting solenoid coil that provides a 1.5 T magnetic field. An iron flux-return located outside the coil is instrumented with resistive plate chambers to detect K_L^0 mesons and muons.

IV. $\Upsilon(2S)$ RECONSTRUCTION

Reconstruction begins with the selection of π^\pm , K^\pm , p/\bar{p} , K_s^0 and π^0 to reconstruct a $\chi_{bJ}(1P)$ candidate. We then select a γ candidate and combine it with the $\chi_{bJ}(1P)$ to form a $\Upsilon(2S)$ candidate.

A. $\chi_{bJ}(1P)$ Reconstruction

The $\chi_{bJ}(1P)$ state can decay to many hadronic final states. For decays into all-charged final states, we focus on the same 26 modes as in Ref. [12]:

$2(\pi^+\pi^-)$, $3(\pi^+\pi^-)$, $4(\pi^+\pi^-)$, $5(\pi^+\pi^-)$, $\pi^+\pi^-K^+K^-$, $2(\pi^+\pi^-)K^+K^-$, $3(\pi^+\pi^-)K^+K^-$, $4(\pi^+\pi^-)K^+K^-$, $2(K^+K^-)$, $\pi^+\pi^-2(K^+K^-)$, $2(\pi^+\pi^-K^+K^-)$, $3(\pi^+\pi^-)2(K^+K^-)$, $\pi^+\pi^-p\bar{p}$, $2(\pi^+\pi^-)p\bar{p}$, $3(\pi^+\pi^-)p\bar{p}$, $4(\pi^+\pi^-)p\bar{p}$, $\pi^+\pi^-K^+K^-p\bar{p}$, $2(\pi^+\pi^-)K^+K^-p\bar{p}$, $3(\pi^+\pi^-)K^+K^-p\bar{p}$, $\pi^\pm K^\mp K_s^0$, $\pi^+\pi^-\pi^\pm K^\mp K_s^0$, $2(\pi^+\pi^-\pi^\pm K^\mp K_s^0)$, $3(\pi^+\pi^-\pi^\pm K^\mp K_s^0)$, $\pi^+\pi^-2K_s^0$, $2(\pi^+\pi^-K_s^0)$, and $3(\pi^+\pi^-)2K_s^0$.

One π^0 is added to the above final states, excluding $2(\pi^+\pi^-)\pi^0$, $3(\pi^+\pi^-)\pi^0$, $4(\pi^+\pi^-)\pi^0$ and $5(\pi^+\pi^-)\pi^0$ as those are forbidden by G-parity conservation [11], resulting in a total of 22 modes reconstructed with one π^0 . An additional 26 modes are reconstructed with the addition of two π^0 's to the charged final states enumerated above.

In total, 74 light hadronic decay modes of the $\chi_{bJ}(1P)$ are reconstructed. Charged particles (π^\pm , K^\pm , p/\bar{p}), K_s^0 and π^0 mesons are selected as follows:

Impact parameters: For charged tracks, we require maximum distances of closest approach with respect to the interaction point (IP), in both the xy transverse plane (dr) and along the z axis ($|dz|$), with the z -axis defined as the direction opposite to the e^+ beam. The selection criteria applied are $dr < 1$ cm and $|dz| < 4$ cm, to ensure that charged tracks are originating from the IP and not the result of beam-wall or beam-gas interactions. These requirements are not imposed on the charged pions arising from a K_s^0 decay.

Number of charged tracks: Selection criteria are also applied to the number of tracks (4, 6, 8, 10, or 12) depending on the mode.

Charged pion and kaon selection: Charged pions and kaons are identified based on their likelihood ratios $\mathcal{L}_{K/\pi} = \frac{\mathcal{L}_K}{\mathcal{L}_K + \mathcal{L}_\pi}$, where \mathcal{L}_K and \mathcal{L}_π are the likelihoods for K^\pm and π^\pm , respectively, calculated using the number of photoelectrons from the ACC, information from the TOF and specific ionization in the CDC. We apply $\mathcal{L}_{K/\pi} < 0.6$ for selecting pions and also require them not to be a daughter of any K_s^0 candidate. Similarly, $\mathcal{L}_{K/\pi} > 0.6$ is used to select kaons. For the above mentioned criteria, the kaon identification efficiency is 81 – 90% with a kaon-to-pion misidentification probability of 9 – 14%. Pions are detected with an efficiency of 91 – 95% with a kaon-to-pion misidentification probability of 8 – 13%.

Selection of p/\bar{p} : protons and antiprotons are identified based on the likelihood ratios $\mathcal{L}_{p/K}$ and $\mathcal{L}_{p/\pi}$. The criteria applied for proton or antiproton selection are: $\mathcal{L}_{p/K} > 0.7$ and $\mathcal{L}_{p/\pi} > 0.7$. The proton identification efficiency is 95%, while the probability of a kaon being misidentified as a proton is below 3%.

K_s^0 selection: Candidate K_s^0 mesons are reconstructed by combining two oppositely charged tracks (pion mass assumed) with an invariant mass between 486 and 509 MeV/ c^2 . The selected candidates are also required to satisfy the criteria described in Ref. [20] to ensure that their decay vertices are displaced from the IP.

π^0 reconstruction: A π^0 is reconstructed from a pair of γ 's, each having energy greater than 100 MeV. The reconstructed π^0 should have an invariant mass within [113, 157] MeV/ c^2 , which is $\pm 3.5\sigma$ around the nominal π^0 mass [21].

B. Transition Photon Selection

Radiative photon candidates arising from the transition $\Upsilon(2S) \rightarrow \gamma\chi_{bJ}(1P)$ are chosen based on the following quantities:

Energy of the photon (E_γ): The signal photon has energy 100 – 240 MeV for $\chi_{b0}(1P)$, 70 – 190 MeV for $\chi_{b1}(1P)$, and 50 – 170 MeV for $\chi_{b2}(1P)$. To cover all three ranges, a lower threshold of 30 MeV is applied on E_γ for selecting the photon.

Polar angle of the γ (θ_γ): We define θ_γ as the angle between the γ direction and the z axis. To reduce the beam background contamination, photons only in the barrel region ($\theta_\gamma \in [0.5, 2.3]$ rad) are retained.

E9/E25: The showers in the ECL have a variety of energy deposition patterns; the variable E9/E25 compares the amount of energy deposited in a 3×3 crystal block (E9) around the crystal with maximum energy to that in a 5×5 crystal block (E25). We apply the criterion $E9/E25 > 0.85$ to select photon candidates.

Charged track match: The photon cluster in the ECL should not match with the trajectories of charged track(s) in the CDC extrapolated into the ECL.

π^0 rejection: The candidate γ should be inconsistent with those arising from the decay of π^0 in the final state.

Selected γ candidates satisfying the above criteria are then combined with the reconstructed $\chi_{bJ}(1P)$ candidate to form an $\Upsilon(2S)$ candidate. At this stage, we apply a very loose requirement on $|\Delta E| < 0.5$ GeV, where ΔE is the difference between the energy of the $\Upsilon(2S)$ candidate and the center-of-mass energy.

C. Continuum Suppression

Continuum background events result from light (u , d , s and c) quark-antiquark pairs produced in e^+e^- collisions. Signal $\chi_{bJ}(1P)$ decay events have a spherical topology, in

contrast to ‘back-to-back’ jetlike continuum events. To suppress the latter, the cosine of the angle between the photon candidate and the thrust axis (calculated from the final state hadrons) in the $\Upsilon(2S)$ rest frame, $\cos\theta_T$, is considered. Signal events have a uniform distribution in this variable while continuum events peak near $|\cos\theta_T| = 1$. A requirement $|\cos\theta_T| < 0.8$ is therefore applied to reduce the continuum background.

V. KINEMATIC FIT AND REDUCED χ^2 CRITERION

In an analysis where all the final state particles are reconstructed, a kinematic fit applying energy-momentum conservation (4C) can be helpful in improving the mass resolution. The reduced χ^2 (χ^2/NDF) from the 4C fit is also used as a selection criterion for signal (and to select the best candidate in cases where multiple candidates are found). After the event selection criteria and continuum suppression described above are imposed, a criterion on the reduced χ^2 is applied for further background suppression.

Optimization for the criterion on the reduced χ^2 is performed for the $\chi_{b0}(1P)$, as it is the signal of interest for the width measurement. The optimization is performed using either (a) sum of the product branching-fractions $\mathcal{B}[\Upsilon(2S) \rightarrow \gamma\chi_{b1}(1P)] \times \mathcal{B}[\chi_{b1}(1P) \rightarrow X_i]$ for 13 modes (available in Ref [11], excluding upper limits), multiplied by the ratio of the sum of signal yields for $\chi_{b0}(1P)$ and $\chi_{b1}(1P)$ in those 13 modes, or (b) the product branching fraction as in case (a), but varied by $\pm 1\sigma$ around the obtained uncertainty. The $\chi_{b0}(1P)$ signal region in terms of $\Delta M \equiv M[\chi_{bJ}(1P)\gamma] - M[\chi_{bJ}(1P)]$ distribution is defined as $[138, 180] \text{ MeV}/c^2$, which corresponds to a $\pm 3\sigma$ window. The non-continuum background contribution is estimated from a data-equivalent MC sample of $\Upsilon(2S)$ decaying generically, in the same mass window.

A figure-of-merit (FOM) is calculated as $S/\sqrt{(S+B)}$, where S (B) is the expected signal (background) yield. The dependence of the FOM on the reduced χ^2 condition is shown in Fig. 1, from which we select a criteria on reduced $\chi^2 < 3$. The FOM is recalculated for the case (b) scenario, and is again shown in Fig. 1. The optimal point remains unchanged.

VI. FIT TO DATA

We use MC simulation to set up an extended unbinned maximum-likelihood fit of the three $\chi_{bJ}(1P)$ ($J = 0, 1, 2$) candidate ΔM distributions. To decide the probability distribution function (PDF) for the signal components, the respective signal MC samples are studied. All three signal shapes are parametrized with the sum of a symmetric and an asymmetric Gaussian function having common mean. The asymmetric component is added to account for low-energy tails. The (three) width param-

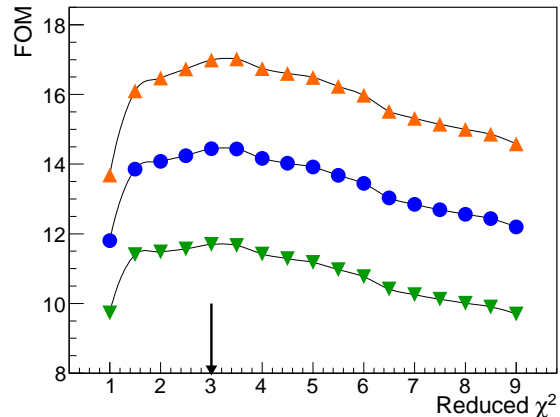


FIG. 1: Variation of the FOM with the reduced χ^2 cut. The FOM is also recalculated by varying the product branching fraction by $\pm 1\sigma$ around its error. The curve with upward orange triangles is for the positive variation, the curve with downward green triangles for the negative variation, whereas the curve with blue circles corresponds to the central value.

eters of the Gaussians are fixed to the MC values for all modes in the fit. The width of the symmetric Gaussians for $\chi_{bJ}(1P)$ ($J = 0, 1, 2$) are found to be $4.6 \pm 0.5 \text{ MeV}$, $4.2 \pm 0.4 \text{ MeV}$ and $4.1 \pm 0.4 \text{ MeV}$, respectively. The parameters for all modes in MC are close and have a small RMS. Therefore, we fix each parameter to its mean value and vary within the RMS to estimate the assorted systematic uncertainty. In order to account for a modest difference in the detector resolution between data and simulations, we apply a calibration factor common to the three signal components. The background is modeled with the sum of an exponential function and a first-order Chebyshev polynomial. The corresponding four parameters (exponent, slope, relative fraction and background yield) are allowed to vary in the fit.

The result of the likelihood fit to the ΔM distributions for the sum of 74 modes in data is shown in Fig. 2; the p -value of the fit is 0.37. The $\chi_{bJ}(1P)$ signal yields are found to be 5 times larger than those obtained in our previous analysis [12]. The masses of the $\chi_{bJ}(1P)$ ($J = 0, 1, 2$) states obtained are in excellent agreement with their world average values [21]. Results are summarized in Table II, including the obtained signal yields in each mode. The resolution calibration factor is found to be 1.13 ± 0.02 , in a reasonable agreement with previous Belle estimates for this correction [12].

TABLE II: $\chi_{bJ}(1P)$ ($J = 0, 1, 2$) masses and yields obtained from the fit to data. (Errors are statistical only.)

Signal	Yield	Mass in MeV/c^2
$\chi_{b0}(1P)$	1197 ± 58	9858.98 ± 0.33
$\chi_{b1}(1P)$	4747 ± 94	9893.05 ± 0.12
$\chi_{b2}(1P)$	3064 ± 87	9911.81 ± 0.16

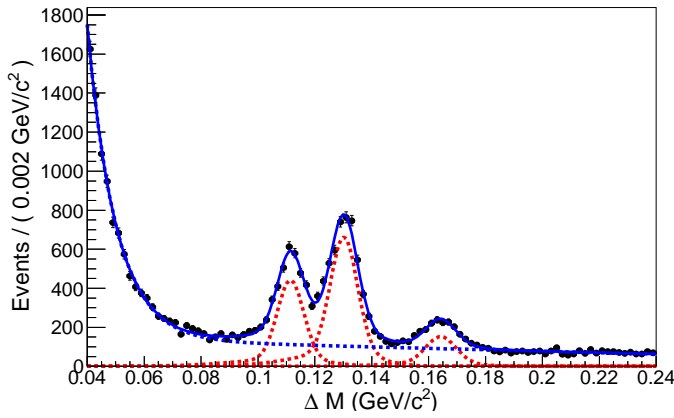


FIG. 2: ΔM distribution in the $\Upsilon(2S)$ data. Black points with error bars are the data; the solid blue and dashed blue curves show the total fit and background components. The three $\chi_{bJ}(1P)$ ($J = 0, 1$, and 2 , respectively from right to left) components are indicated by the red dashed curves.

A. Mode Selection

With signal shapes, including means, fixed in the fit to the result obtained from the sum of 74 modes (described previously), we fit the ΔM distribution in each individual mode to determine its significance as $\sqrt{-2 \ln(\mathcal{L}_0/\mathcal{L}_{\max})}$, where \mathcal{L}_0 (\mathcal{L}_{\max}) is the likelihood value when the signal yield is fixed to zero (allowed to vary). In total, 41 modes have above 5 standard deviation (σ) significance in at least one of the $\chi_{bJ}(1P)$ ($J = 0, 1, 2$) signals. The ΔM distribution in those 41 modes is shown in Figs. 3–8.

B. Branching Fraction Results

The major source of systematic uncertainty is due to the effect of possible intermediate decays (mentioned in Section II) on the signal reconstruction efficiency. The deviation in efficiency relative to the default phase space assumption is 2 – 23%. Uncertainties on the signal yield due to PDF shapes are estimated by varying the shape parameters fixed in the nominal fit by $\pm 1\sigma$, and are found to be in the range 3 – 12%. The uncertainty due to the limited size of the signal MC sample is 1%. Uncertainties associated with photon detection (3%), charged track reconstruction (0.35% per track), particle identification (1.5 – 4.5%), K_S^0 reconstruction (2.2% per K_S^0), π^0 reconstruction (2.2% per π^0), and the number of $\Upsilon(2S)$ in data sample (2.3%) are also taken into account. Systematic errors are added in quadrature mode by mode, and sum to between 6% and 27%.

The product branching fractions, $\mathcal{B}[\Upsilon(2S) \rightarrow \gamma \chi_{bJ}(1P)] \times \mathcal{B}[\chi_{b1}(1P) \rightarrow X_i]$, for each $\chi_{bJ}(1P)$ decay having significance exceeding 3σ , are listed in Table III along with the corresponding statistical significance. In case of significance lower than 3σ , we obtain an upper limit at 90% confidence level (CL) on the

branching fraction (\mathcal{B}_{UL}) by integrating the likelihood (\mathcal{L}) of the fit with fixed values of the branching fraction: $\int_0^{\mathcal{B}_{\text{UL}}} \mathcal{L}(\mathcal{B}) d\mathcal{B} = 0.9 \times \int_0^1 \mathcal{L}(\mathcal{B}) d\mathcal{B}$. Systematic uncertainties in \mathcal{B}_{UL} are included by convolving the likelihood function with a Gaussian function with a width equal to the total uncertainty. Our branching fraction results are consistent with, and more precise than, those reported in CLEO’s analysis. Furthermore, a $\chi_{bJ}(1P)$ signal for $J = 0, 1$, and 2 has been observed for the first time in 9, 27, and 16 modes, respectively. And, we also found first evidence of a $\chi_{bJ}(1P)$ signal in 18, 1, and 14 modes for $J = 0, 1$, and 2 , respectively.

VII. $\chi_{b0}(1P)$ WIDTH MEASUREMENT

As mentioned in Section I, the $\chi_{b0}(1P)$ width may be above 2 MeV, but no experimental measurement thus far has been attempted. The large signal yield obtained in our branching fraction studies of the $\chi_{bJ}(1P)$ triplet motivates a width measurement of the $\chi_{b0}(1P)$. For this study, we select the 41 significant modes described in Section VI B. We obtain signal shape parameters from our high statistics MC sample, for which the signal yield is 5 times the value observed for each mode in data. For fitting this MC sample each signal component is parameterized by a sum of a symmetric and an asymmetric Gaussian with common mean. The two widths of the asymmetric Gaussian and the fraction between the two Gaussians are identical for all the three signal components.

For the $\chi_{b0}(1P)$ width measurement in data, we model the three signals as described above for MC case, except for the $\chi_{b0}(1P)$, for which the sum of two Gaussian functions is convolved with a Breit-Wigner function. The symmetric part is convolved using the Voigtian function of RooFit [22], whereas the asymmetric Gaussian function is convolved numerically using the FFTW (Fastest Fourier Transform in the West) [23] package of ROOT, with the same Breit-Wigner function whose width is floated. Individual widths of the symmetric Gaussians for all three signals are fixed to the corresponding MC values, and are multiplied by a common resolution-correction factor to take account of possible data-MC difference. An unbinned extended maximum likelihood fit is performed in data to the ΔM distribution for the sum of the 41 modes having high significance. All background parameters components are floated, whereas all signal parameters are fixed to the MC-fit values except for their individual mean and yield, and the resolution-correction factor. Figure 9 shows the result of the fit on data. The $\chi_{b0}(1P)$ width is found to be 1.3 ± 0.9 MeV. In the absence of a statistically significant result, we derive an upper limit on the width (see below).

The systematic uncertainty due to the fixed PDF parameters is ± 0.2 MeV. To estimate uncertainty due to the assumption of negligible $\chi_{b2}(1P)$ width, a non-zero width (0.5 MeV) to $\chi_{b2}(1P)$ is introduced and this affects

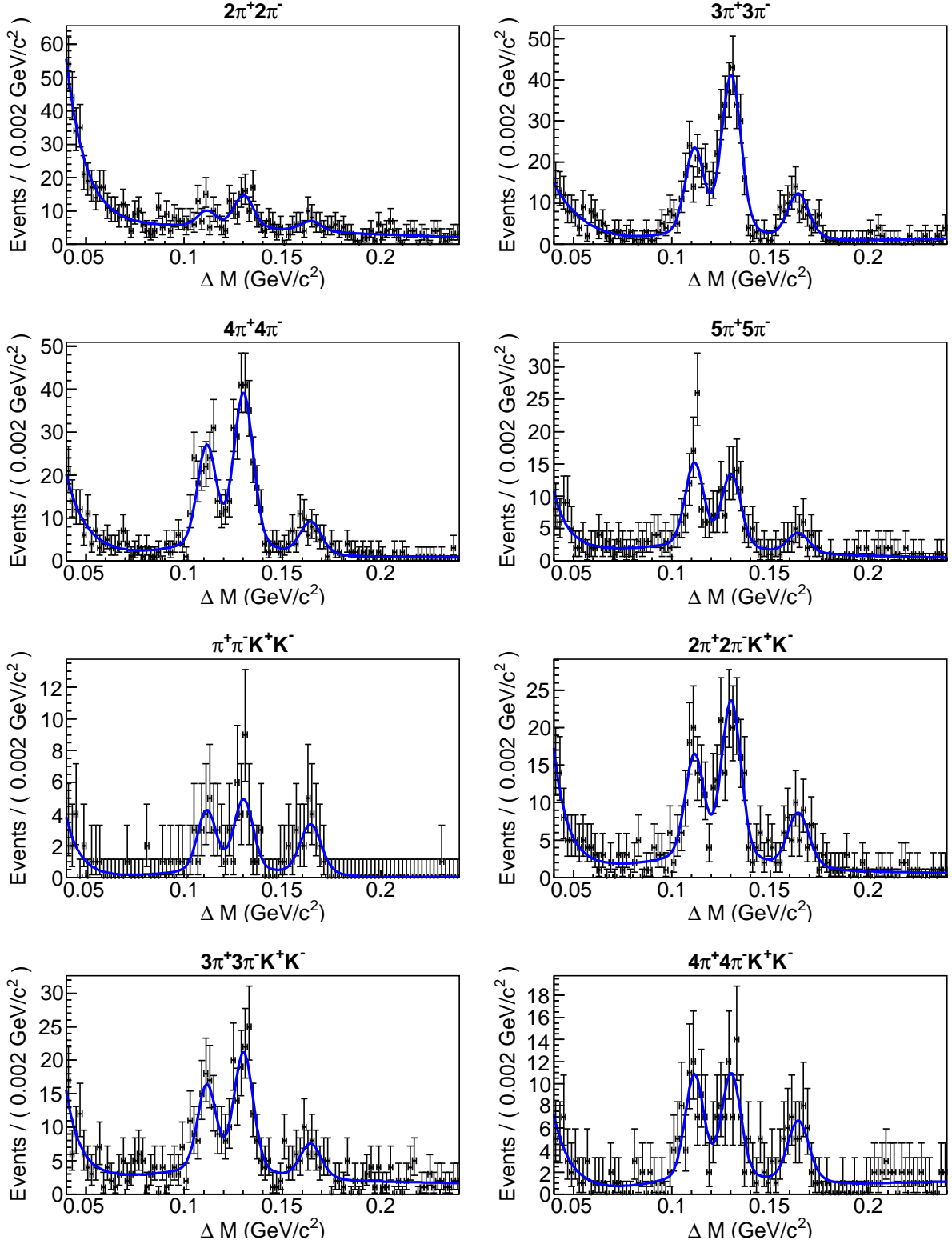


FIG. 3: ΔM distributions in $\Upsilon(2S)$ data for $2(\pi^+\pi^-)$, $3(\pi^+\pi^-)$, $4(\pi^+\pi^-)$, $5(\pi^+\pi^-)$, $\pi^+\pi^-K^+K^-$, $2(\pi^+\pi^-)K^+K^-$, $3(\pi^+\pi^-)K^+K^-$, and $4(\pi^+\pi^-)K^+K^-$ final states. Black dots with error bars are data and the blue curves represent the total fit result.

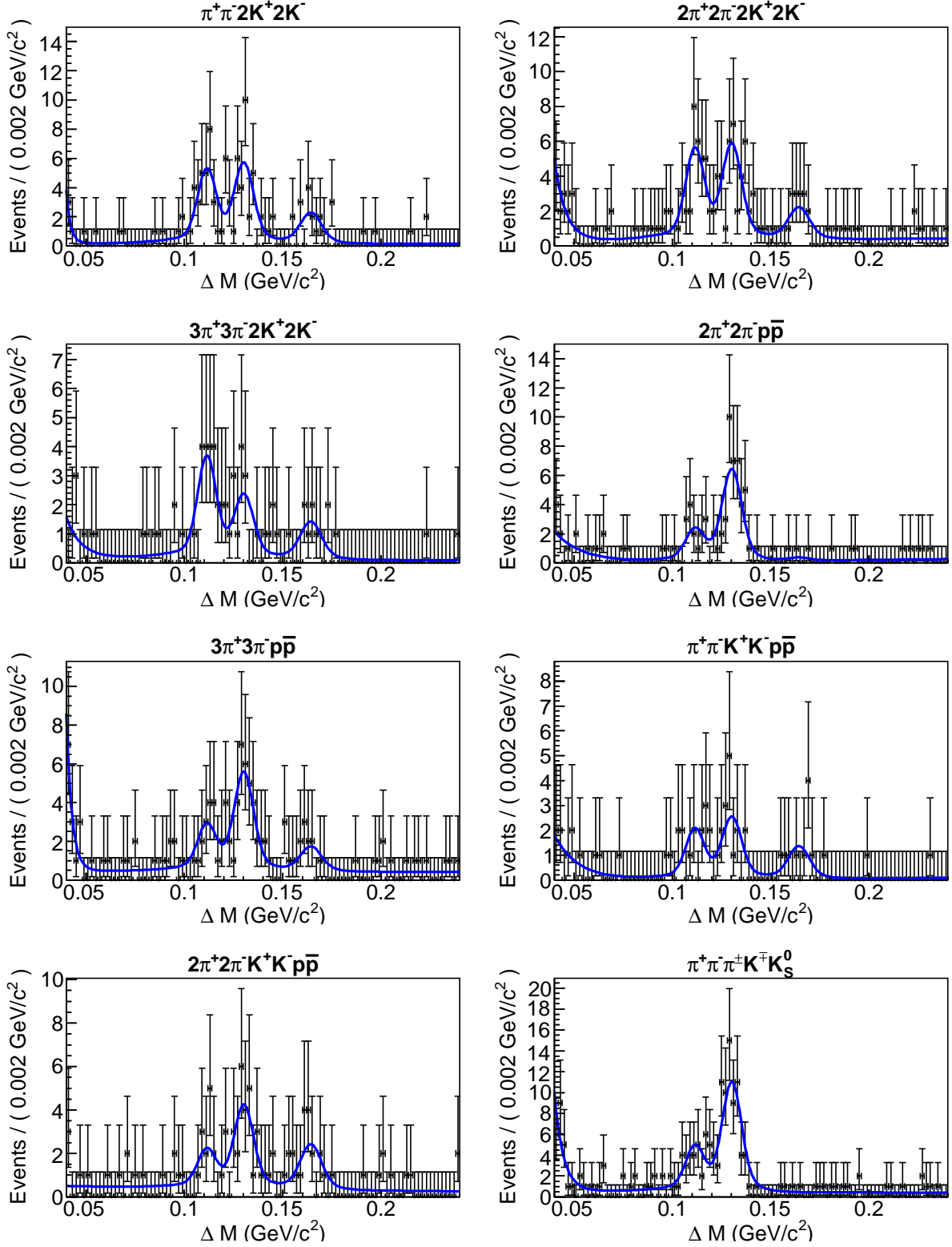


FIG. 4: ΔM distributions in $\Upsilon(2S)$ data for $\pi^+\pi^-2(K^+K^-)$, $2(\pi^+\pi^-K^+K^-)$, $3(\pi^+\pi^-)2(K^+K^-)$, $2(\pi^+\pi^-)p\bar{p}$, $3(\pi^+\pi^-)p\bar{p}$, $\pi^+\pi^-K^+K^-p\bar{p}$, $2(\pi^+\pi^-)K^+K^-p\bar{p}$, and $\pi^+\pi^-\pi^+K^-K_S^0$ final states. Black dots with error bars are data and the blue curves represent the total fit result.

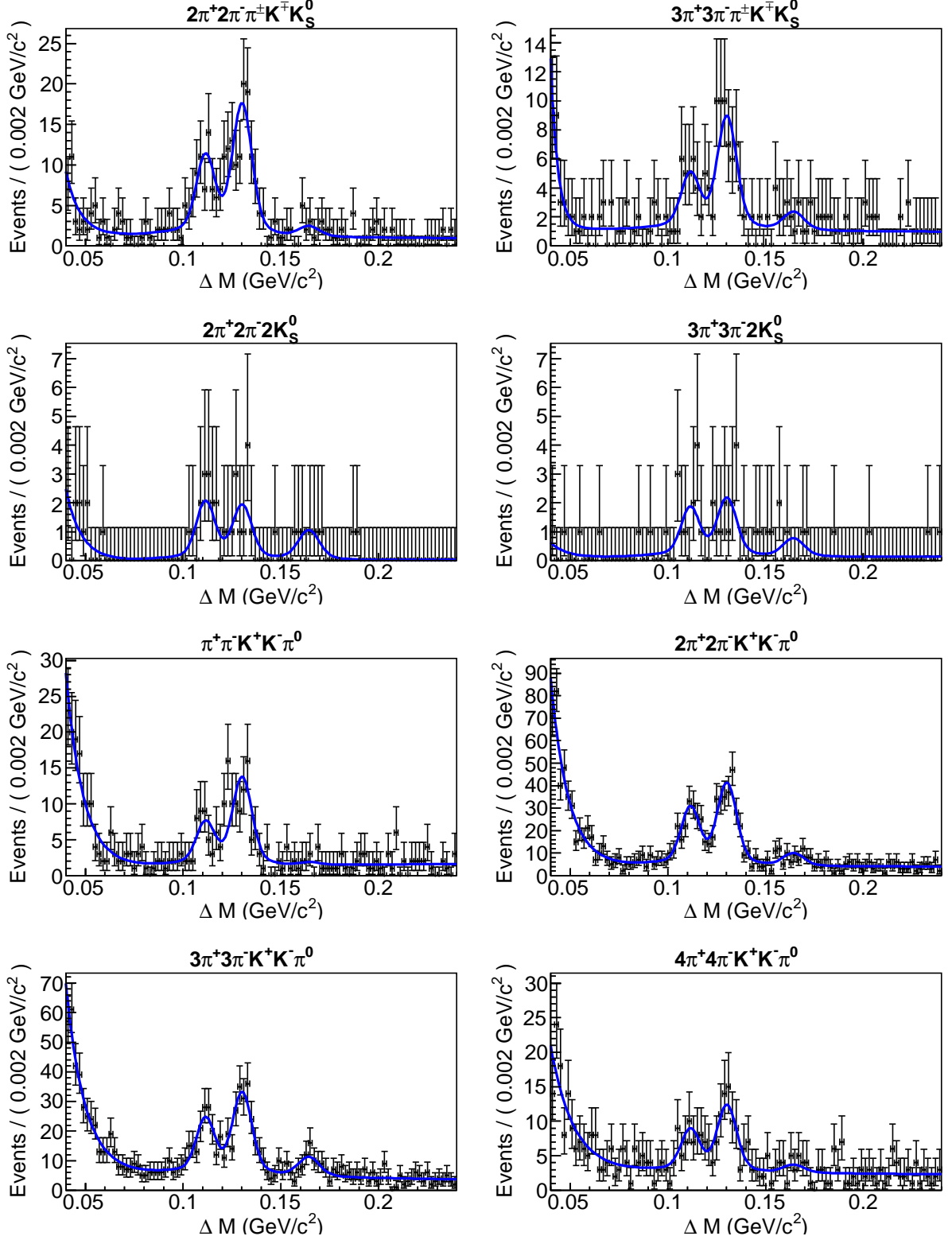


FIG. 5: ΔM distributions in $\Upsilon(2S)$ data for $2(\pi^+\pi^-)\pi^\pm K^\mp K_S^0$, $3(\pi^+\pi^-)\pi^\pm K^\mp K_S^0$, $2(\pi^+\pi^-)K_S^0$, $3(\pi^+\pi^-)2K_S^0$, $\pi^+\pi^-K^+K^-\pi^0$, $2(\pi^+\pi^-)K^+K^-\pi^0$, $3(\pi^+\pi^-)K^+K^-\pi^0$ and $4(\pi^+\pi^-)K^+K^-\pi^0$ final states. Black dots with error bars are data and the blue curves represent the total fit result.

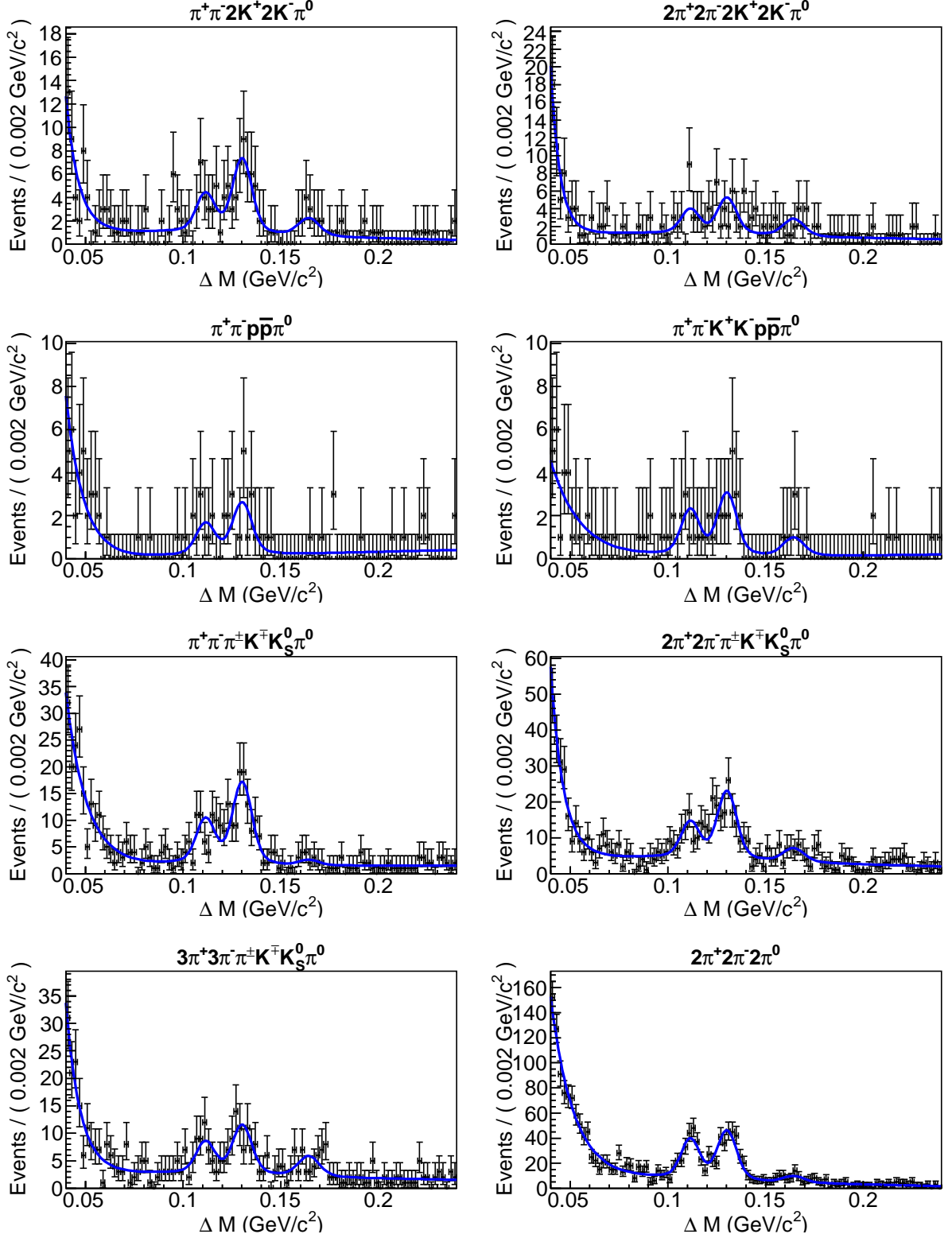


FIG. 6: ΔM distributions in $\Upsilon(2S)$ data for $\pi^+\pi^-2(K^+K^-\pi^0)$, $2(\pi^+\pi^-K^+K^-\pi^0)$, $\pi^+\pi^-p\bar{p}\pi^0$, $\pi^+\pi^-K^+K^-\bar{p}p\pi^0$, $\pi^+\pi^-\pi^\pm K^\mp K_S^0\pi^0$, $2(\pi^+\pi^-\pi^\pm K^\mp K_S^0\pi^0)$, $3(\pi^+\pi^-\pi^\pm K^\mp K_S^0\pi^0)$ and $2(\pi^+\pi^-)2\pi^0$ final states. Black dots with error bars are data and the blue curves represent the total fit result.

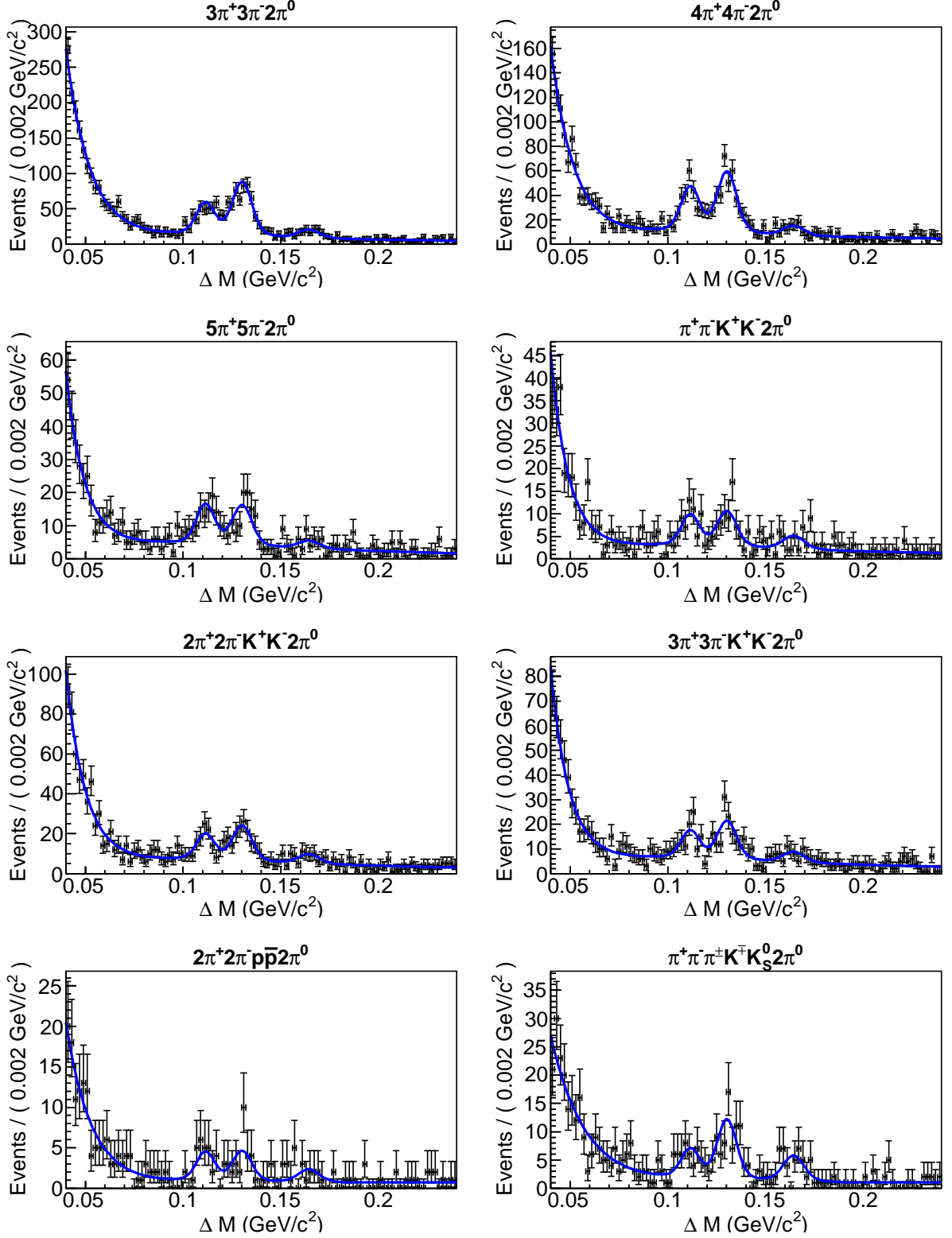


FIG. 7: ΔM distributions in $\Upsilon(2S)$ data for $3(\pi^+\pi^-)2\pi^0$, $4(\pi^+\pi^-)2\pi^0$, $5(\pi^+\pi^-)2\pi^0$, $(\pi^+\pi^-)K^+K^-2\pi^0$, $2(\pi^+\pi^-)K^+K^-2\pi^0$, $3(\pi^+\pi^-)K^+K^-2\pi^0$, $2(\pi^+\pi^-)p\bar{p}2\pi^0$ and $\pi^+\pi^-\pi^+K^-K^02\pi^0$ final states. Black dots with error bars are data and the blue curves represent the total fit result.

TABLE III: Product branching fractions $\mathcal{B}[\Upsilon(2S) \rightarrow \gamma\chi_{bJ}(1P)] \times \mathcal{B}[\chi_{b1}(1P) \rightarrow h_i]$ ($\times 10^{-5}$) and statistical significance for each $\chi_{bJ}(1P)$ ($J = 0, 1, 2$) state. Upper limits at the 90% CL are calculated for modes having significance less than 3σ . The values indicated by the symbol represent the first observation or evidence of signal in that mode.

Mode	$\chi_{b0}(1P)$		$\chi_{b1}(1P)$		$\chi_{b2}(1P)$	
	\mathcal{B}	σ	\mathcal{B}	σ	\mathcal{B}	σ
$2\pi^+2\pi^-$	$0.13 \pm 0.05 \pm 0.02$	3.0	$0.31 \pm 0.06 \pm 0.04$	6.8	$0.15 \pm 0.06 \pm 0.02$	3.1
$3\pi^+3\pi^-$	$0.67 \pm 0.08 \pm 0.06$	11.0	$1.84 \pm 0.12 \pm 0.16$	23.6	$0.96 \pm 0.10 \pm 0.10$	12.6
$4\pi^+4\pi^-$	$0.78 \pm 0.13 \pm 0.11$	8.5	$2.8 \pm 0.2 \pm 0.4$	22.5	$1.8 \pm 0.2 \pm 0.2$	14.6
$5\pi^+5\pi^-$	$0.53 \pm 0.14 \pm 0.10$	4.9	$1.5 \pm 0.2 \pm 0.3$	10.8	$1.7 \pm 0.2 \pm 0.3$	10.9
$\pi^+\pi^-K^+K^-$	$0.15 \pm 0.03 \pm 0.03$	8.1	$0.17 \pm 0.03 \pm 0.03$	8.6	$0.15 \pm 0.04 \pm 0.03$	6.3
$2\pi^+2\pi^-K^+K^-$	$0.53 \pm 0.08 \pm 0.05$	8.7	$1.20 \pm 0.11 \pm 0.10$	16.3	$0.8 \pm 0.10 \pm 0.08$	11.5
$3\pi^+3\pi^-K^+K^-$	$0.6 \pm 0.13 \pm 0.06$	5.8	$1.7 \pm 0.2 \pm 0.2$	13.7	$1.2 \pm 0.2 \pm 0.1$	9.8
$4\pi^+4\pi^-K^+K^-$	$1.2 \pm 0.2 \pm 0.2$	7.9	$1.6 \pm 0.2 \pm 0.2$	10.5	$1.6 \pm 0.2 \pm 0.2$	9.6
$\pi^+\pi^-2K^+2K^-$	$0.18 \pm 0.05 \pm 0.02$	5.4	$0.35 \pm 0.06 \pm 0.03$	8.6	$0.32 \pm 0.07 \pm 0.03$	7.4
$2\pi^+2\pi^-2K^+2K^-$	$0.33 \pm 0.12 \pm 0.03$	4.4	$0.60 \pm 0.12 \pm 0.06$	7.8	$0.56 \pm 0.12 \pm 0.06$	7.2
$3\pi^+3\pi^-2K^+2K^-$	$0.33 \pm 0.12 \pm 0.04$	3.8	$0.42 \pm 0.14 \pm 0.06$	4.5	$0.7 \pm 0.2 \pm 0.1$	6.2
$2\pi^+2\pi^-p\bar{p}$	< 0.2	0.9	$0.51 \pm 0.08 \pm 0.06$	10.2	$0.16 \pm 0.06 \pm 0.03$	3.5
$3\pi^+3\pi^-p\bar{p}$	$0.23 \pm 0.1 \pm 0.03$	3.1	$0.70 \pm 0.14 \pm 0.08$	7.8	$0.31 \pm 0.11 \pm 0.04$	3.6
$\pi^+\pi^-K^+K^-p\bar{p}$	$0.13 \pm 0.04 \pm 0.02$	4.2	$0.18 \pm 0.05 \pm 0.03$	5.7	$0.15 \pm 0.05 \pm 0.03$	3.7
$2\pi^+2\pi^-K^+K^-p\bar{p}$	$0.31 \pm 0.10 \pm 0.05$	4.5	$0.4 \pm 0.1 \pm 0.1$	6.3	$0.2 \pm 0.08 \pm 0.03$	3.4
$\pi^+\pi^-\pi^\pm K^\mp K_S^0$	< 0.1	0.0	$0.7 \pm 0.1 \pm 0.1$	12.9	$0.28 \pm 0.07 \pm 0.05$	5.0
$2\pi^+2\pi^-\pi^\pm K^\mp K_S^0$	< 0.4	2.2	$1.9 \pm 0.2 \pm 0.2$	13.9	$1.1 \pm 0.2 \pm 0.1$	8.5
$3\pi^+3\pi^-\pi^\pm K^\mp K_S^0$	< 0.7	2.1	$1.6 \pm 0.3 \pm 0.1$	8.9	$0.8 \pm 0.2 \pm 0.1$	4.3
$2\pi^+2\pi^-2K_S^0$	$0.2 \pm 0.08 \pm 0.04$	4.2	$0.28 \pm 0.08 \pm 0.03$	5.4	$0.29 \pm 0.09 \pm 0.03$	5.2
$3\pi^+3\pi^-2K_S^0$	< 0.6	2.2	$0.5 \pm 0.2 \pm 0.1$	5.0	$0.4 \pm 0.2 \pm 0.1$	3.8
$\pi^+\pi^-K^+K^-\pi^0$	< 0.2	0.7	$0.77 \pm 0.10 \pm 0.06$	10.7	$0.36 \pm 0.09 \pm 0.04$	5.2
$2\pi^+2\pi^-K^+K^-\pi^0$	$0.8 \pm 0.2 \pm 0.2$	4.5	$4.2 \pm 0.3 \pm 0.7$	18.3	$2.8 \pm 0.3 \pm 0.5$	11.8
$3\pi^+3\pi^-K^+K^-\pi^0$	$1.8 \pm 0.4 \pm 0.4$	5.2	$6 \pm 0.6 \pm 1.1$	14.5	$3.8 \pm 0.5 \pm 0.7$	9.0
$4\pi^+4\pi^-K^+K^-\pi^0$	< 1.7	1.4	$4 \pm 0.7 \pm 1.0$	7.8	$2.4 \pm 0.6 \pm 0.6$	4.4
$\pi^+\pi^-2K^+2K^-\pi^0$	$0.28 \pm 0.11 \pm 0.04$	3.2	$0.9 \pm 0.2 \pm 0.2$	7.9	$0.45 \pm 0.15 \pm 0.08$	3.9
$2\pi^+2\pi^-2K^+2K^-\pi^0$	$0.7 \pm 0.3 \pm 0.1$	3.2	$1.1 \pm 0.3 \pm 0.2$	5.0	$0.7 \pm 0.3 \pm 0.1$	3.5
$\pi^+\pi^-p\bar{p}\pi^0$	< 0.1	0.0	$0.24 \pm 0.07 \pm 0.04$	5.4	$0.14 \pm 0.06 \pm 0.02$	3.3
$\pi^+\pi^-K^+K^-p\bar{p}\pi^0$	< 0.5	2.8	$0.5 \pm 0.1 \pm 0.2$	5.5	$0.32 \pm 0.13 \pm 0.12$	3.3
$\pi^+\pi^-\pi^\pm K^\mp K_S^0\pi^0$	< 0.5	1.5	$2.2 \pm 0.3 \pm 0.2$	11.9	$1.2 \pm 0.2 \pm 0.2$	6.1
$2\pi^+2\pi^-\pi^\pm K^\mp K_S^0\pi^0$	$1.3 \pm 0.4 \pm 0.2$	3.8	$5.3 \pm 0.6 \pm 0.8$	12.1	$2.6 \pm 0.5 \pm 0.5$	6.1
$3\pi^+3\pi^-\pi^\pm K^\mp K_S^0\pi^0$	$2.4 \pm 0.7 \pm 0.5$	4.1	$4.6 \pm 0.8 \pm 1.0$	7.6	$2.9 \pm 0.7 \pm 0.6$	4.7
$2\pi^+2\pi^-2\pi^0$	$0.8 \pm 0.2 \pm 0.2$	3.9	$4.5 \pm 0.4 \pm 1$	16.9	$3.4 \pm 0.3 \pm 0.8$	12.5
$3\pi^+3\pi^-2\pi^0$	$3.6 \pm 0.6 \pm 0.5$	6.7	$16.8 \pm 0.9 \pm 2.3$	24.0	$9.7 \pm 0.9 \pm 1.5$	13.6
$4\pi^+4\pi^-2\pi^0$	$4.8 \pm 1 \pm 1.0$	5.3	$22.3 \pm 1.5 \pm 4.7$	19.6	$15.5 \pm 1.5 \pm 3.3$	13.3
$5\pi^+5\pi^-2\pi^0$	< 5.1	2.6	$10.8 \pm 1.6 \pm 2.4$	8.4	$11 \pm 1.9 \pm 2.5$	7.1
$\pi^+\pi^-K^+K^-2\pi^0$	$0.5 \pm 0.2 \pm 0.1$	3.3	$1.1 \pm 0.2 \pm 0.3$	7.0	$0.9 \pm 0.2 \pm 0.2$	5.4
$2\pi^+2\pi^-K^+K^-2\pi^0$	$1.7 \pm 0.5 \pm 0.4$	3.9	$4.9 \pm 0.6 \pm 1.1$	10.0	$3.5 \pm 0.6 \pm 0.8$	6.8
$3\pi^+3\pi^-K^+K^-2\pi^0$	$3.2 \pm 1 \pm 0.8$	3.6	$8.9 \pm 1.2 \pm 2.2$	9.4	$6.4 \pm 1.2 \pm 1.6$	6.3
$2\pi^+2\pi^-p\bar{p}2\pi^0$	< 1.8	2.7	$1.8 \pm 0.5 \pm 0.3$	5.0	$1.6 \pm 0.5 \pm 0.3$	4.4
$\pi^+\pi^-\pi^\pm K^\mp K_S^02\pi^0$	$2.0 \pm 0.5 \pm 0.3$	5.1	$3.6 \pm 0.5 \pm 0.4$	8.6	$1.7 \pm 0.5 \pm 0.2$	4.2
$2\pi^+2\pi^-\pi^\pm K^\mp K_S^02\pi^0$	$3.0 \pm 1.0 \pm 0.6$	3.5	$9 \pm 1.3 \pm 1.7$	9.1	$5.1 \pm 1.2 \pm 1.0$	5.1

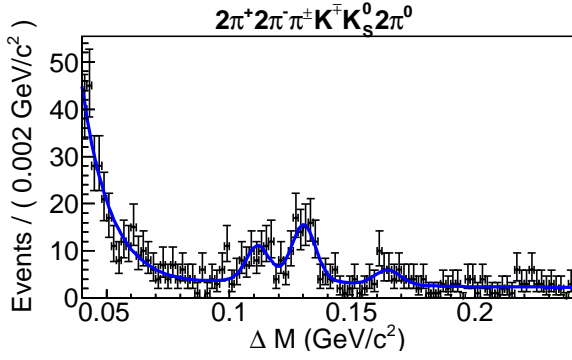


FIG. 8: ΔM distributions in $\Upsilon(2S)$ data for $2(\pi^+\pi^-)\pi^\pm K^\mp K_S^0 2\pi^0$ final state. Black dots with error bars are data and the blue curve represents the total fit result.

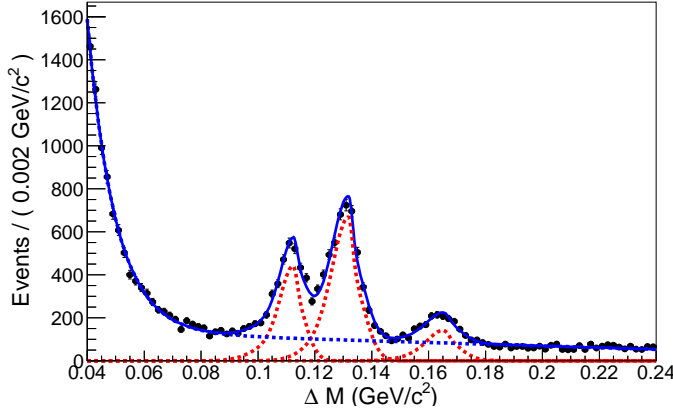


FIG. 9: Result of maximum likelihood fit for width measurement to the ΔM distribution in sum of 41 modes. Black points with error bars are the data; blue solid and blue dashed curves are total fit and background components. The three $\chi_{bJ}(1P)$ components are indicated by the red dashed curve.

$\chi_{b0}(1P)$ width by ± 0.1 MeV. We generate a large ensemble of pseudo-experiments for different $\chi_{b0}(1P)$ width hypotheses using the PDF parameters obtained from data, and perform a linearity test between the generated and fitted width values. An uncertainty of ± 0.1 MeV is assigned to account for possible deviation from linearity. We obtain a 90% CL upper limit on the width of the $\chi_{b0}(1P)$ ($\mathcal{W}_{\text{limit}}$) by integrating the likelihood (\mathcal{L}) of the fit using fixed values of the width: $\int_0^{\mathcal{W}_{\text{limit}}} \mathcal{L}(\mathcal{W}) d\mathcal{W} = 0.9 \times \int_0^\infty \mathcal{L}(\mathcal{W}) d\mathcal{W}$. Systematic uncertainties are included by convolving the likelihood function with a Gaussian function of width equal to the total systematic uncertainty. We estimate the width of the $\chi_{b0}(1P) < 2.4$ MeV.

VIII. SUMMARY

We have studied $\chi_{bJ}(1P)$ states produced from the $\Upsilon(2S)$ via electric dipole radiative transition, decaying to

light hadronic final states. Our measurements are consistent with, and more precise than, those reported by the CLEO Collaboration [11]. We also report a $\chi_{bJ}(1P)$ signal for $J = 0, 1$, and 2 for the first time in 27, 28, and 30 modes, respectively. Furthermore, in the absence of a statistically significant result, a 90% confidence-level upper limit is set on the $\chi_{b0}(1P)$ width at $\Gamma_{\text{total}} < 2.4$ MeV.

Acknowledgments

We thank the KEKB group for the excellent operation of the accelerator; the KEK cryogenics group for the efficient operation of the solenoid; and the KEK computer group, the National Institute of Informatics, and the PNNL/EMSL computing group for valuable computing and SINET4 network support. We acknowledge support from the Ministry of Education, Culture, Sports, Science, and Technology (MEXT) of Japan, the Japan Society for the Promotion of Science (JSPS), and the Tau-Lepton Physics Research Center of Nagoya University; the Australian Research Council; Austrian Science Fund under Grant No. P 22742-N16 and P 26794-N20; the National Natural Science Foundation of China under Contracts No. 10575109, No. 10775142, No. 10875115, No. 11175187, No. 11475187 and No. 11575017; the Chinese Academy of Science Center for Excellence in Particle Physics; the Ministry of Education, Youth and Sports of the Czech Republic under Contract No. LG14034; the Carl Zeiss Foundation, the Deutsche Forschungsgemeinschaft, the Excellence Cluster Universe, and the VolkswagenStiftung; the Department of Science and Technology of India; the Istituto Nazionale di Fisica Nucleare of Italy; the WCU program of the Ministry of Education, National Research Foundation (NRF) of Korea Grants No. 2011-0029457, No. 2012-0008143, No. 2012R1A1A2008330, No. 2013R1A1A3007772, No. 2014R1A2A2A01005286, No. 2014R1A2A2A01002734, No. 2015R1A2A2A01003280, No. 2015H1A2A1033649; the Basic Research Lab program under NRF Grant No. KRF-2011-0020333, Center for Korean J-PARC Users, No. NRF-2013K1A3A7A06056592; the Brain Korea 21-Plus program and Radiation Science Research Institute; the Polish Ministry of Science and Higher Education and the National Science Center; the Ministry of Education and Science of the Russian Federation and the Russian Foundation for Basic Research; the Slovenian Research Agency; Ikerbasque, Basque Foundation for Science and the Euskal Herriko Unibertsitatea (UPV/EHU) under program UFI 11/55 (Spain); the Swiss National Science Foundation; the Ministry of Education and the Ministry of Science and Technology of Taiwan; and the U.S. Department of Energy and the National Science Foundation. This work is supported by a Grant-in-Aid from MEXT for Science Research in a Priority Area (“New Development of Flavor Physics”) and from JSPS for Creative Scientific

-
- [1] L. V. Landau, Dokl. Akad. Nauk. **60**, 207 (1948); C. N. Yang, Phys. Rev. D **77**, 242 (1950).
 - [2] W. Kwong, J. L. Rosner, and C. Quigg, Ann. Rev. Nucl. Part. Sci. **37**, 325 (1987).
 - [3] J. Segovia, P. G. Ortega, D. R. Entem and F. Francisco, Phys. Rev. D **93**, 074027 (2016).
 - [4] C. W. Hwang and R. S. Guo, Phys. Rev. D **82**, 034021 (2010).
 - [5] G. L. Wang, Phys. Lett. B **653**, 206 (2007).
 - [6] G. L. Wang, Phys. Lett. B **674**, 172 (2009).
 - [7] J. T. Lavery, S. F. Radford, and W. W. Repko, arXiv:0901.3917v3 [hep-ph].
 - [8] D. Ebert, R. N. Faustov, and V. O. Galkin, Phys. Rev. D **67**, 014027 (2003).
 - [9] S. N. Gupta, J. M. Johnson, and W. W. Repko, Phys. Rev. D **54**, 2075 (1996).
 - [10] S. Godfrey and N. Isgur, Phys. Rev. D **32**, 189 (1985).
 - [11] D. M. Asner *et al.* (CLEO Collaboration), Phys. Rev. D **78**, 091103(R) (2008).
 - [12] S. Sandilya *et al.* (Belle Collaboration), Phys. Rev. Lett. **111**, 112001 (2013).
 - [13] C. Patrignani *et al.*, Ann. Rev. Nucl. Part. Sci. **63**, 21 – 44 (2013).
 - [14] X. L. Wang *et al.* (Belle Collaboration), Phys. Rev. D **84**, 071107(R) (2011).
 - [15] A. Abashian *et al.* (Belle Collaboration), Nucl. Instrum. Methods Phys. Res., Sect. A **479**, 117 (2002); also, see the detector section in J. Brodzicka *et al.*, Prog. Theor. Exp. Phys., 04D001 (2012).
 - [16] S. Kurokawa and E. Kikutani, Nucl. Instrum. Methods Phys. Res., Sect. A **499**, 1 (2003), and other papers included in this volume; T. Abe *et al.*, Prog. Theor. Exp. Phys., 03A001 (2013) and following articles up to 03A011.
 - [17] M. Jacob and G. C. Wick, Annals Phys. **7**, 404 (1959); Annals Phys. **281**, 774 (2000).
 - [18] E. Barberio and Z. Was, Comput. Phys. Commun. **79**, 291 (1994); P. Golonka and Z. Was, Eur. Phys. J. C **45**, 97 (2006); P. Golonka and Z. Was, Eur. Phys. J. C **50**, 53 (2007).
 - [19] T. Sjöstrand *et al.*, Comput. Phys. Commun. **178**, 852 (2008).
 - [20] K.-F. Chen *et al.* (Belle Collaboration), Phys. Rev. D **72**, 012004 (2005).
 - [21] K. A. Olive *et al.* (Particle Data Group), Chin. Phys. C **38**, 090001 (2014).
 - [22] W. Verkerke, and D. P. Kirkby, arXiv:physics/0306116.
 - [23] <http://www.fft.w.org/#documentation>